Journal of
Manufacturing and Materials Processing

MDPI

Article

Analysis of Surface Grinding of Thermoplastics Specimens with Inline Measurements

Roberto Spina [1,2,3,*], Bruno Melo Cavalcante [1,2], Maria Grazia Guerra [1] and Marco Massari [4]

[1] Dipartimento di Meccanica, Matematica e Management, Politecnico di Bari, 70125 Bari, Italy; bruno.melocavalcante@poliba.it (B.M.C.); mariagrazia.guerra@poliba.it (M.G.G.)
[2] Istituto Nazionale di Fisica Nucleare (INFN)—Sezione di Bari, 70125 Bari, Italy
[3] Consiglio Nazionale Delle Ricerche—Istituto di Fotonica e Nanotecnologie (CNR-IFN), 70125 Bari, Italy
[4] Bosch—Tecnologie Diesel S.p.A., 70026 Modugno, Italy; marco.massari2@it.bosch.com
* Correspondence: roberto.spina@poliba.it; Tel.: +39-080-5963228

Abstract: This paper analyzes the surface grinding of unfilled and glass-filled polyamides. The process is performed by varying the workpiece velocities to evaluate applied practical applications in the industry while being energy efficient. During the machining, the temperatures, normal forces, tangential forces, and spindle power were collected, and the surface quality was evaluated by a scanning electron microscope (SEM), helping to determine material removal mechanisms and study their behavior under grinding. One of the primary outcomes of the present research was that, different from most metallic and ceramic materials, polyamides benefited from the material removal rate increase. We had higher quality material removed efficiently. Also, the specific energy of both materials converged to previously demonstrated values, showing once again that it is highly dependent on the matrix. Moreover, the time-dependent mechanical properties of the material during processing were identified. The fast application of the force at high speed gave less time to respond to the mechanical strain, determining an improvement in the surface quality of the samples. Consequently, the surface quality of the final product improved with a speed increase, leading to low roughness values.

Keywords: grinding; thermoplastics; measurements

Citation: Spina, R.; Cavalcante, B.M.; Guerra, M.G.; Massari, M. Analysis of Surface Grinding of Thermoplastics Specimens with Inline Measurements. *J. Manuf. Mater. Process.* **2022**, *6*, 81. https://doi.org/10.3390/jmmp6040081

Academic Editor: Mark J. Jackson

Received: 15 July 2022
Accepted: 29 July 2022
Published: 2 August 2022

1. Introduction

The surface conditions of a component broadly influence its properties, such as haptics, optics, tribology, and its lifetime. Therefore, the proper judgment of expected machined surfaces is crucial in designing and manufacturing high-quality parts [1]. The surface improvement of polymer matrix composites (PMCs) is focused on the study of carbon and glass fiber reinforced plastics (CFRPs and GFRPs) [2–4]. Process signatures are thus required for these materials to evaluate the interactions between the internal material loads in manufacturing processes and the resulting material modifications, allowing a deeper and more comprehensive understanding of the correlations between machining mechanisms and parameters, surface properties, and surface integrity [5]. The surface improvement from grinding is essential concerning other machining processes, especially when PMCs parts are realized with Additive Manufacturing.

Grinding involves an increased risk of thermal damage to the machined workpieces due to high temperatures and larger contact zones compared to other manufacturing processes such as milling and turning [6]. In the case of polymers, a grinding limit is the glass transition temperature T_g, defined as a temperature at which the polymer changes from a rigid glassy material to a soft one. If this threshold is passed, the material resistance changes with a reduction of the mechanical properties, requiring coolant in the tool-workpiece contact zone to shorten undesired effects [7]. Heat generation is critical because dimensional and shape accuracy decreases due to thermal deformation and grinding burn. Usually

optimized in metals, the process allows for avoiding burnings and defects on the workpiece surface. Optimal results are achieved by accurately monitoring the temperature during grinding, using conventional or innovative techniques [8]. Dry machining provides a valid alternative [9], but it exposes fibers and accumulated chips during processing [10], with the risk of grinding wheel blockage [11]. The use of large grinding depths (>300 µm) without coolant is usually used to validate the results of the thermal simulations [12]. Cutting with large grinding depths, combined with low velocities, is not productive because an increase in the production of large batches occurs. Low coolant flow rates are desired to face strict ecological and economic requirements without lowering process reliability and worsening workpiece quality. A free jet flow can break through the air barrier caused by the rotation of the grinding wheel [13].

The T_g not only limits the use of thermoplastics during processing, but the temperature control is highly desired to achieve acceptable results [14]. Changes in surface and subsurface properties during grinding are linked to processing parameters and quantities. Due to missing information on the internal material loads, such as stresses, strains, temperature values, or gradients, a reasonable selection of machining parameters to achieve a desired surface integrity state is not always possible [15]. The viscous deformation of a polymer also plays a decisive role in determining the quality of a machined surface. To minimize the surface roughness, the machining conditions should be selected so that the material removal deformation in the regime falls without viscoplastic scaling/tearing and brittle cracking [16]. This condition is typically implemented with thermoplastics by working below T_g and employing moderate cutting depths and conventional refrigeration. If the temperatures are under control, the whole system provides high efficiency and high surface quality [17]. However, there is a need for large material removal since multiple grinding passes can be applied, assuring the benefits of lower cutting depths [6].

This paper aims to evaluate the resulting surface properties of natural and glass fiber-filled polyamides (PA66 and PA66GF30) after the surface grinding process was performed by varying the workpiece velocities to determine whether this process can be applied practically in the industry while being energy efficient. During the machining, the temperatures, normal forces, tangential forces, and spindle power were collected, and the surface quality was evaluated by a scanning electron microscope (SEM), helping to determine material removal mechanisms and study their behavior under grinding.

2. Materials and Methods

2.1. Sample Production

Rough samples were milled from a plate of dimensions 6 × 500 × 3000 mm^3 produced with extruded TECAMID® PA66 and PA66GF30 provided by Ensinger GmbH (Nufrigen, Germany). These samples were reduced to a dimension of 5 × 30 × 60 mm^3 and drilled in the center to fit a thermocouple. The hole diameter was 1.5 mm, while its depth was 29.5 mm. Table 1 reports the machining parameters to realize the samples. These parameters were selected after significant preliminary testing leading to free-defect specimens, following the machining guidelines suggested by the supplier for this class of materials. Dimensions of the milled specimens before grinding were measured using a digital micrometer with a resolution of 1 µm. The ground surface of 5 × 60 mm^2 was opposite the hole entrance. Sixty mm was a sufficient path length to acquire enough data for high workpiece speeds while having a small area to concentrate the normal and tangential forces. This condition was essential for an adequate reading of the forces during grinding for materials with low elastic moduli. The specimen height of 30 mm avoided machining the sensor's tip while giving enough stock material to normalize the ground surface before sensor readings.

Table 1. Machining parameters.

Property	Value	Unit
Milling		
Tool Diameter	100	mm
Tool Speed	900	rpm
Feed Speed	1000	mm/min
Drilling		
Tool Diameter	1.5	mm
Tool Speed	1400	rpm

The thermomechanical properties of the investigated materials, as provided by the supplier, are summarized in Table 2.

Table 2. Main properties of the TECAMID materials (from supplier datasheets).

Property	PA66	PA66GF30	
	Value		Unit
General			
Material class	PA66	PA66	-
Reinforcement (glass fiber)	0	30	%
Physical			
Density ρ	1.15	1.34	g/cm^3
Glass transition temperature T_g	47	48	°C
Melting (Softening) temperature T_m	258	254	°C
Thermal conductivity k	0.36	0.39	W/(K × m)
Thermal diffusivity α	0.20	0.24	mm^2/s
Water absorption (24 h/96 h @ 23 °C)	0.2/0.4	0.1/0.2	%
Mechanical (Tensile test)			
Young's modulus E	3500	5500	MPa
Yield tensile strength σ_Y	84	91	MPa
Ultimate tensile strength σ_R	85	91	MPa
Elongation at break $A\%$	9.6	2.1	%
Coefficient of thermal expansion α_{CTE}	120	50	µm/m/°C

Since polyamides were susceptible to property variation due to environmental conditions, the samples were tested using differential scanning calorimetry (DSC) to check for any T_g variation from supplier data [17]. Analysis was performed on small samples (5 mg) with a DSC 403 F3 Pegasus (Netzsch-Gerätebau GmbH, Selb, Germany), equipped with a silver furnace, setting up a thermal cycle from −50 to 340 °C at a heating/cooling rate of 20 °C/min and N_2 condition.

2.2. Grinding Setup and Sensors

The prerequisite for a technological signature of grinding was the thermo-mechanical load characterization during processing. An inline measurement system of forces and temperatures was implemented on an industrial computerized numerical control (CNC) machine with a specialized setup (Figure 1). A Planomat 408 CNC machine (Blohm Jung GmbH, Hamburg, Germany) was improved using a SINUMERIK 840d sl control (Siemens AG, Munich, Germany) with a Data Acquisition (DAQ) system capable of spindle power registration at a sampling of 0.002 s. The maximum machine spindle limits were 1450 rpm and 7.5 kW. Two Slimline cells (Kistler Group AG, Winterthur, Switzerland) were added to measure the normal and tangential forces. A MAXYMOS TYP5877A/B (Kistler Group AG, Winterthur, Switzerland) acquired the cell signals, working as an amplifier and monitoring

system, with a sampling of 0.001 s. The applied filter was 5 Hz. A Type K-thermocouple (1.0 mm diameter and 500 mm length) measured processing temperatures up to 1200 °C.

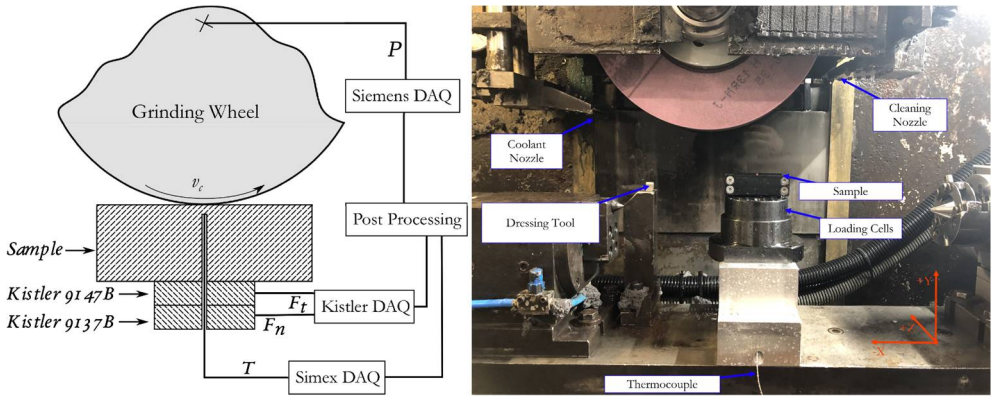

Figure 1. Sensor diagram and the internal configuration of the grinding machine.

A Multicon CMC-99 controller (Simex Sp. z o.o, Gdansk, Poland) recorded the logged data of the thermocouple with a sampling interval of 0.1 s. The temperature sensor's tip was 29.5 mm far from the bottom surface, and the hole was filled with epoxy resin to prevent measurement errors derived from movements of the sensor axis. The temperature and the power were filtered post-processing after the data acquisition was completed.

A stationary 0.6 × 0.6 × 5 mm^3 diamond plate, equipped with three tips, allowed the dressing of the wheel with a low-pressure coolant with oil emulsion CIMCOOLCIMTECH A31F (Cimcool Industrial Products B.V., Vlaardingen, NL, USA) plus water at 3.5% in volume. The grinding machine had two cooling nozzles. The first nozzle was oriented to the contact point between the wheel and workpiece for controlling temperatures during machining. The second nozzle, oriented to the wheel rear, cleaned the grinding wheel of debris accumulated in the porous structure, causing possible non-cutting and temperature rises. Furthermore, the two cooling settings were low pressure (3 bar) and high pressure (6 bar). The aluminum oxide Al_2O_3 grain wheel was selected based on previous experience with the same materials [11]. The wheel was coded as 45A120-5G11RM-LV233/35 (ELBE Schleifmittelwerk GmBh & Co KG, Sachsenheim, Germany) and had an initial diameter D equal to 400 mm and a thickness t of 30 mm. Table 3 reports the dressing parameters employed during experiments.

Table 3. Dressing Parameters.

Property	Value	Unit
Grinding wheel speed v_c	40	m/s
Dressing quota in Y	0.036	mm
Z-axis speed	120	mm/min
Number of passes	1	-
Coolant pressure	3	bar

After every process step, surface quality was evaluated to observe the microscopic alterations on the samples. Firstly, the pieces were cleaned and mounted after processing on an Evo MA25 Scanning Electronic Microscope (Carl Zeiss AG, Oberkochen, Germany) to examine the ground surface and systematically appraise the surface quality and possible factors of defects. The ground surface was coated with gold to reveal the initial microstructure without polishing it to alter the surface quality. The surface images were taken with 20 kV using a Back Scattered Electron (BSE) detector to identify backscattered electrons under very low angles and a maximum magnification of 500× [18]. In the case of undamaged parts, the surface roughness was then measured using a MarSurf XCR20 surface contour and roughness unit (Mahr GmbH, Göttingen, Germany). This instrument had a resolution

of 0.19 µm using the 175 mm probe arm and 0.04 µm relative to the measuring system, using a mechanical probe MFW250 at a speed of 0.5 mm/s and a measuring distance of L_s equal to 3.2 mm in a normal direction to the grinding path. The principal surface quality parameters were the arithmetic mean height R_a and the maximum height parameter R_z, according to definitions of ISO 21920-2:2021. R_a and R_z were sampled by the unity analysis PGK120 integrated with the instrument, automatically filtering the results and presenting a surface profile.

3. Results and Discussion

3.1. Initial Considerations

After rough milling and drilling the plate to realize the samples, the top cutting surface was evaluated to assess the quality before grinding. The machined PA66 samples had a R_a of 4.2 µm and an R_z of 20.4 µm, while the corresponding values for the machined PA66GF30 samples were 7.2 µm and 40.1 µm, respectively. A higher roughness of the PA66GF30 samples was expected because of the presence of the fibers. Five infeed velocities v_w were chosen to observe the effects of this parameter on the cutting zone, endeavoring to increase the temperature influence by reducing the Peclet number P_e, defined as:

$$P_e = \frac{v_w \times l_g}{4 \times \alpha} \tag{1}$$

with α, the material's thermal diffusivity, and the length l_g,

$$l_g = \sqrt{a_e \times D} \tag{2}$$

Defined as the geometrical contact length between the tool and the workpiece. Its value determined the amount of heat transferred to the workpiece due to the diffusive effects compared to the advective effects [19]. A Peclet number is a similarity number, characterizing the cutting regime's relative influence on the workpiece material's thermal properties. For P_e greater than 10, the heat source (the cutting tool) moves over the workpiece faster than the velocity of thermal wave propagation. The thermal energy generated in cutting due to the plastic deformation of the work material and friction at the tool-chip interface did not affect the work material ahead of the tool. On the contrary, for P_e less than 10, the thermal energy due to the plastic deformation and friction makes an essential contribution to the process of plastic deformation during cutting, affecting the mechanical properties of the work material [20]. The contact time t_c was

$$t_c = \frac{l_g}{v_w} \tag{3}$$

defined as the time the tool was in contact with the workpiece. Its value ranged between 0.211 and 0.632 s for a contact length l_g of 6.32 mm. As the speed increased, less heat was transferred to the samples because of a reduction in the contact time. In the case of polyamide samples, the coolant flow was sufficient to avoid significant thermal variations. The low thermal diffusivity value combined with the proposed speeds led to situations where the Peclet number P_e in this application was higher, in the range 60–200, than most conventional grinding operations on metals, making the advective effects dominant [21]. The contact zone was not expected to increase as the values of v_w were much less dominant to the process than the cutting speed v_c. In the fastest scenario with v_w equal to 1800 mm/min, the grinding wheel speed v_c was three orders greater than the infeed speed v_w, making a micrometrical growth in the geometric contact zone. The grinding parameters are presented in Table 4.

Table 4. Grinding Parameters.

Property	Value	Unit
Grinding wheel speed v_c	30	m/s
Cutting depth a_e	0.1	mm
Infeed speed v_w	600, 900, 1200, 1500, 1800	mm/min
Grinding thickness b	5	mm
Coolant pressure p_c	6	bar

3.2. Forces and Energy Evaluation

The maximum values of the normal force F_n and tangential force F_t measured by the loading cells during processing are shown in Figure 2. These values were collected after stabilization, making three repetitions of grinding with the same processing parameters. Previous experience suggested that the lubricant could influence the obtained values, and in this case, the nozzle angle and flow rate were adjusted to minimize interference during data acquisition [17]. Normal and tangential forces on both materials tended to increase as the infeed speed v_w grew. This behavior agreed with previous works in PMCs [2,12], revealing small tangential forces with low infeed speeds. The material removal rate Q, defined as

$$Q = b \times a_e \times v_w \tag{4}$$

increased with the cutting depth a_e and infeed speed v_w, making larger values easily measured. A cutting depth increase generated high forces combined with a good measurement of temperature and power. However, using this technique proved to cause much debris in the grinding wheel requiring constant dressing. This condition was very unfavorable for a productive reality, and the infeed speed was increased until practically measuring the forces correctly. The cutting power P on the surface was the product of the measured tangential force F_t, normal force F_n, the grinding wheel speed $v_{c,}$ and the normal radial speed v_n,

$$P = F_t \times v_c + F_n \times v_{\mathrm{n}} \tag{5}$$

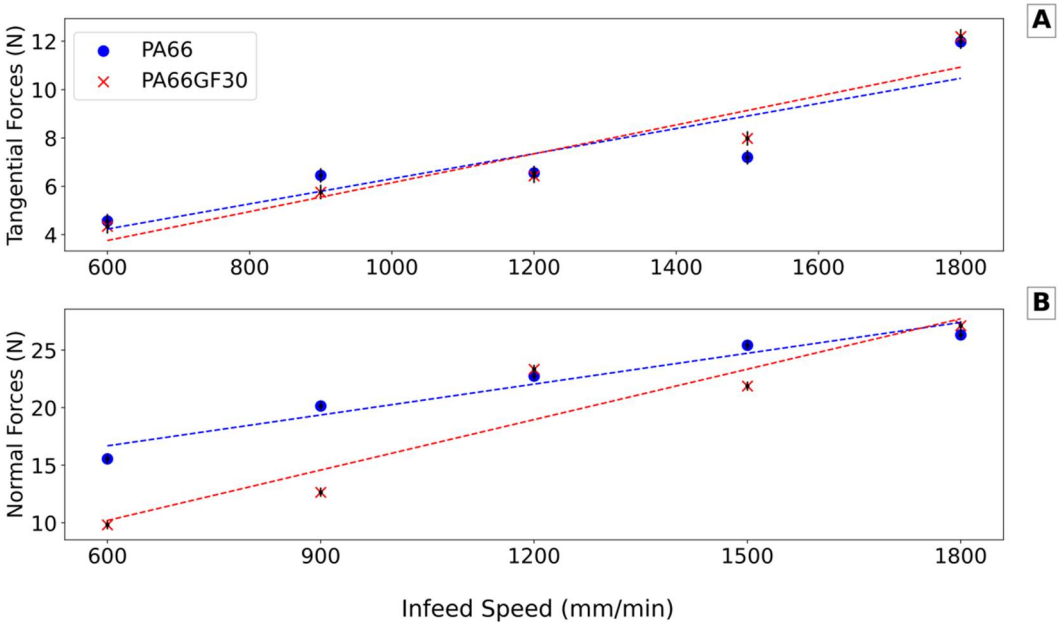

Figure 2. (**A**) Measured tangential forces F_t and (**B**) measured normal force F_n.

Since v_n was equal to zero for surface grinding, P was only the product of F_t and v_c. This power was directly compared to the measured spindle power $P_{spindle}$, defining the energy cutting partition η as

$$\eta = \frac{P}{P_{spindle}} \tag{6}$$

The values of the power and force were taken at the same point as the temperature measurement made by the thermocouple. The energy cutting partition η measured how much energy was directly transferred to cutting the workpiece. A η reduction suggested an increase in wasted energy. Analyzing the process, three main phases existed. The rubbing phase occurred at small depths with elastic deformations at the surface of the workpiece. Plowing was accomplished by some material becoming plastically deformed with a depth increase. This plastic deformation typically presented itself in the form of upheaval around the leading edge of the grain, and it was most often characterized by the formation of a scratch or groove. Finally, at yet more significant depths, a chip was formed and ejected from the workpiece surface [22]. Power was lost during the grinding process primarily by heat generated on the surface by rubbing and plastic deformation. The secondary loss was the mechanical energy for chip removal. The specific energy e_s was computed from the valuable part of the mechanical energy.

$$e_s = \frac{P}{Q} = \frac{F_t \times v_c}{b \times a_e \times v_w} \tag{7}$$

The knowledge of specific energy was essential in grinding because it influenced the surface integrity of machined components in ductile materials. The specific grinding energy was a helpful process parameter to control ductility since the specific grinding energy was accompanied by a transition from ductile-regime to brittle-regime [23]. It indicated how much energy was used to remove one cubic millimeter of material. The value of e_s was typically material-dependent [6]. Figure 3 shows how the infeed speed v_w affected the process efficiency in grinding both materials.

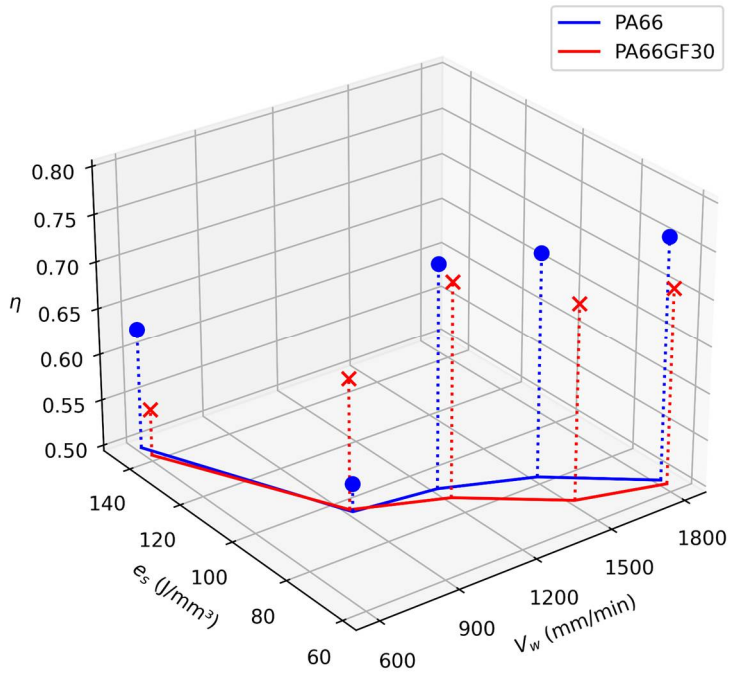

Figure 3. The plot of the specific energy e_s, energy cutting partition η, and infeed speed v_w.

The energy cutting partition η quickly raised with a speed increase, starting from the initial value of 55%, and arriving at the maximum value of 75%. Since the temperature was

not a factor directly involved in the process analysis, the outcome was that high degrees of lost power 1-η at low speeds were explicitly related to mechanical phenomena. A high P_e coupled with conventional refrigeration promoted the thermal dissipation of the generated heat directly to the grinding wheel-coolant system. The results pointed out that the specific energy e_s at a low infeed speed v_w of 900 mm/min was subject to an immediate sharp decline of 28% from the previous value of 600 mm/min. At the highest infeed speed v_w of 1800 mm/min, the required energy to remove one cubic millimeter of material was reduced by more than a half of that at 600 mm/min. The converging specific energy e_s matched other experiences with these materials [17].

Of particular interest was that η and e_s of both materials converged to similar values. This behavior could be attributed to the cutting mechanisms at different infeed speeds. In low infeed speeds, the applied forces in the unfilled material allowed a full plastic deformation and then breaking for the chip formation. The PA66GF30 was more brittle, and less energy was required to remove a fraction of the material. Adding the glass fibers to the PA66 matrix improved mechanical properties such as elastic modulus, yield strength, and ultimate tensile strength, drastically reducing the elongation at break (Table 2). Consequently, a lower cutting force was required to grind the material, as reported in previous research [17]. With an infeed speed increase, forces were applied on the PA66 sample in less time, and the process became more efficient with less energy required to remove material.

3.3. Surface Quality Results

The thermo-mechanical loads applied during grinding modified the surface part integrity. The processing parameters directly influenced the combined load. A higher cutting velocity usually increased the tool-workpiece temperatures while the forces remained stable or decreased due to thermal softening. On the contrary, the tool wear increased the process forces, surface load, and process temperatures by frictional heat [24]. However, the faster the workpiece moved during grinding, the less time the tool was in contact with the workpiece at the same point. The slower the piece moved, the wheel passed more times at the same point, increasing smoothness.

The above-described phenomena partially diverged in the case of the grinding of polymeric materials. As Figure 4 shows, the surface quality of the natural PA66, represented by R_a and R_z, advanced with the increase of the infeed speed v_w. On the contrary, PA66GF30 material presented a slight growth in surface roughness, with less influence of the infeed speed on the final workpiece quality. The R_z values of PA66GF30 samples were within 2.30 µm (low speed) and 3.30 µm (high speed), while the R_z values of PA66 were within 3.51 µm (high speed) and 7.74 µm (low speed). All R_a and R_z values were lower than those of the milled samples. The arithmetic roughness R_a followed the same trend, with the values reduced from 1.0 µm to 0.5 µm for PA66 and between 0.4 µm and 0.6 µm for PA66GF30. The above results suggested the hypothesis of the time-dependent mechanical properties of the material.

The fast application of the force gave less time to respond to the mechanical strain, determining an improvement in the surface quality of the samples. At a low strain rate, the material presented a typical viscoelastic response with a delayed deformation and stress relaxation, while at a high strain rate, the behavior was ideally plastic. The material stiffness changed suddenly with strain rate, probably due to the chain relaxation. The chain motion kept up with the strain rate at low values, causing more significant deformation while presenting minor deformation at a higher rate [25]. The stress-strain relationship and high strain rates caused higher flow stress but more softening. An increasing trend in the maximum stress was associated with increased strain rates [26].

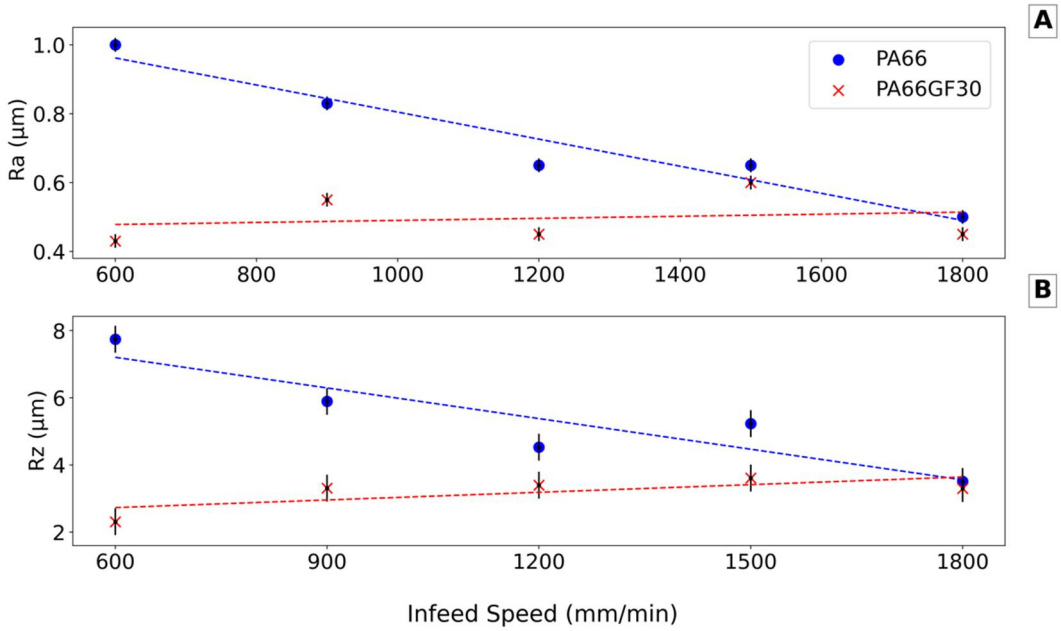

Figure 4. (**A**) The arithmetic mean height R_a and (**B**) the maximum height parameter R_z.

The SEM analysis also confirmed the time-dependent mechanical properties of the material. In Figure 5, the ground surfaces of both materials are shown with a 300× magnification. In the PA66 surfaces, nerving as vestiges of long plastic deformation were present on the surfaces at low infeed speed v_w. With a speed increase, the surfaces were less nerving and smoother, revealing some defects for not perfect cutting. As for the PA66GF30, the fibers did not seem to protrude from the surface at low speeds. Instead, the fibers tended to break with speed growth because of the higher strain rate. In both materials, incomplete cuts caused material accumulation.

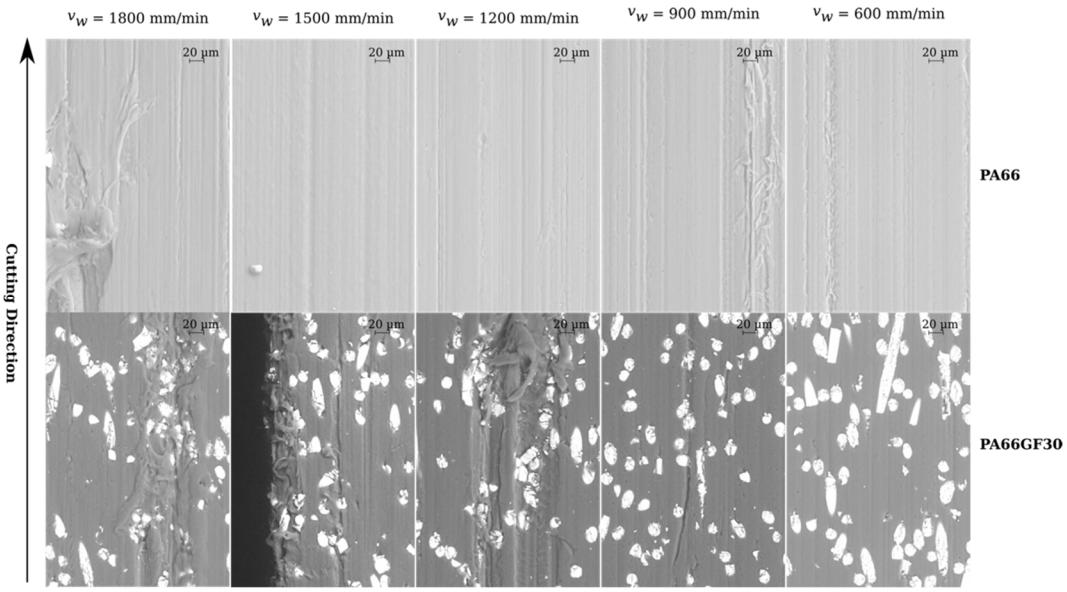

Figure 5. SEM images of the ground surface at 300× amplification.

4. Conclusions

In this study, an energy approach was used to analyze the surface grinding and to consider the effects of infeed speed on the final surface quality of unfilled (PA66) and glass-filled polyamides (PA66GF30). The first result identified the time-dependent mechanical

properties of the material during processing. The fast application of the force gave less time to respond to the mechanical strain, determining an improvement in the surface quality of the samples. The material acted as a viscoelastic response at a low strain rate, while the behavior was ideal plastic at a high strain rate. The specific energy decreased, and the energy cutting partition increased with an increase of the infeed speed, converging to the same values for both materials.

Furthermore, the resulting roughness (arithmetic and maximum height) of PA66 improved with infeed speed, reaching its lowest at the highest speed due to process-induced material brittleness. In the case of PA66GF30, the roughness remained stable in the investigated infeed range, with a slight increase with an infeed increase. These results were also confirmed by the image analysis of the ground surfaces with a scanning electronic microscope.

Further research should be addressed to investigate the morphology of the ground surface, considering the grinding wheel grit size and structure to identify the active grit number and distribution. This way, a surface-focused process control could be implemented to digitally evaluate the grinding process before experimentation and real application in industrial cases.

Author Contributions: Conceptualization, B.M.C., M.G.G. and R.S.; methodology, B.M.C.; validation, M.G.G.; formal analysis, R.S.; investigation, B.M.C. and M.M.; resources, M.M.; data curation, B.M.C.; writing—original draft preparation, B.M.C. and R.S.; writing—review and editing, R.S.; supervision, R.S. and M.M. All authors have read and agreed to the published version of the manuscript.

Funding: This research received no external funding.

Institutional Review Board Statement: Not applicable.

Informed Consent Statement: Not applicable.

Data Availability Statement: Data available on request.

Acknowledgments: The authors thank Luigi Galantucci of Politecnico di Bari, Roberto Rutigliano, Michele Mastropasqua, Antonio Caputo e Saverio Cascella of Tecnologie Diesel S.p.A., for their precious suggestions and support.

Conflicts of Interest: The authors declare that they have no conflict of interest.

References

1. Hockauf, R.; Böß, V.; Grove, T.; Denkena, B. Prediction of Ground Surfaces by Using the Actual Tool Topography. *J. Manuf. Mater. Process.* **2019**, *3*, 40. [CrossRef]
2. Inoue, H.; Kawaguchi, I. Study on the Grinding Mechanism of Glass Fiber Reinforced Plastics. *J. Eng. Mater. Technol.* **1990**, *112*, 341–345. [CrossRef]
3. Hu, N.; Zhang, L. A study on the grindability of multidirectional carbon fibre-reinforced plastics. *J. Mater. Process. Technol.* **2003**, *140*, 152–156. [CrossRef]
4. Huang, Y.; Liu, S.; Xiao, G.; He, Y.; Wang, W. Experimental investigation into the effects of adhesion wear on belt grinding of glass fiber reinforced plastics. *Int. J. Adv. Manuf. Technol.* **2020**, *109*, 463–473. [CrossRef]
5. Brinksmeier, E.; Meyer, D.; Heinzel, C.; Lübben, T.; Sölter, J.; Langenhorst, L.; Frerichs, F.; Kämmler, J.; Kohls, E.; Kuschel, S. Process Signatures—The Missing Link to Predict Surface Integrity in Machining. *Procedia CIRP* **2018**, *71*, 3–10. [CrossRef]
6. Klocke, F. *Manufacturing Processes 2: Grinding, Honing, Lapping*; Springer: Berlin/Heidelberg, Germany, 2010; ISBN 3642100767.
7. Sasahara, H.; Kikuma, T.; Koyasu, R.; Yao, Y. Surface grinding of carbon fiber reinforced plastic (CFRP) with an internal coolant supplied through grinding wheel. *Precis. Eng.* **2014**, *38*, 775–782. [CrossRef]
8. Ito, Y.; Kita, Y.; Fukuhara, Y.; Nomura, M.; Sasahara, H. Development of In-Process Temperature Measurement of Grinding Surface with an Infrared Thermometer. *J. Manuf. Mater. Process.* **2022**, *6*, 44. [CrossRef]
9. Hanasaki, S.; Fujiwara, J.; Tashiro, T. Study on Surface Grinding of Unidirectional Carbon Fiber Reinforced Plastics in Dry Method. In Proceedings of the International Conference on Leading Edge Manufacturing in 21st Century: LEM21, Niigata, Japan, 3–6 November 2003; pp. 297–302. [CrossRef]
10. Ahmad, J. Health and safety aspects in machining FRPs. In *Machining of Polymer Composites*; Springer Science & Business Media: Berlin, Germany, 2009; pp. 293–307. [CrossRef]
11. Spina, R.; Cavalcante, B. Thermal Analysis of PA66 Grinding. *Procedia Manuf.* **2020**, *47*, 910–914. [CrossRef]

12. Kodama, H.; Okazaki, S.; Jiang, Y.; Yoden, H.; Ohashi, K. Thermal influence on surface layer of carbon fiber reinforced plastic (CFRP) in grinding. *Precis. Eng.* **2020**, *65*, 53–63. [CrossRef]
13. Schumski, L.; Guba, N.; Espenhahn, B.; Stöbener, D.; Fischer, A.; Meyer, D. Characterization of the Interaction of Metalworking Fluids with Grinding Wheels. *J. Manuf. Mater. Process.* **2022**, *6*, 51. [CrossRef]
14. Spina, R.; Cavalcante, B. Evaluation of grinding of unfilled and glass fiber reinforced polyamide 6,6. *Polymers* **2020**, *12*, 2288. [CrossRef]
15. Kolkwitz, B.; Kohls, E.; Heinzel, C.; Brinksmeier, E. Correlations between Thermal Loads during Grind-Hardening and Material Modifications Using the Concept of Process Signatures. *J. Manuf. Mater. Process.* **2018**, *2*, 20. [CrossRef]
16. Xiao, K.; Zhang, L. The role of viscous deformation in the machining of polymers. *Int. J. Mech. Sci.* **2002**, *44*, 2317–2336. [CrossRef]
17. Spina, R.; Cavalcante, B.; Massari, M.; Rutigliano, R. Forces and Specific Energy of Polyamide Grinding. *Materials* **2021**, *14*, 5041. [CrossRef]
18. Jawahir, I.; Brinksmeier, E.; M'Saoubi, R.; Aspinwall, D.; Outeiro, J.; Meyer, D.; Umbrello, D.; Jayal, A. Surface integrity in material removal processes: Recent advances. *CIRP Ann.* **2011**, *60*, 603–626. [CrossRef]
19. Malkin, S.; Guo, C. Thermal Analysis of Grinding. *CIRP Ann.* **2007**, *56*, 760–782. [CrossRef]
20. Astakhov, V.P. Machining of Hard Materials—Definitions and Industrial Applications. In *Machining of Hard Materials*; Davim, J., Ed.; Springer: London, UK, 2011. [CrossRef]
21. Barczak, L.; Batako, A.; Morgan, M. A study of plane surface grinding under minimum quantity lubrication (MQL) conditions. *Int. J. Mach. Tools Manuf.* **2010**, *50*, 977–985. [CrossRef]
22. Doman, D.A.; Bauer, R.; Warkentin, A. Experimentally validated finite element model of the rubbing and ploughing phases in scratch tests. *Proc. Inst. Mech. Eng. Part B J. Eng. Manuf.* **2009**, *223*, 1519–1527. [CrossRef]
23. Balogun, V.A.; Edem, I.F.; Adekunle, A.A.; Mativenga, P.T. Specific energy based evaluation of machining efficiency. *J. Clean. Prod.* **2016**, *116*, 187–197. [CrossRef]
24. Stampfer, B.; González, G.; Gerstenmeyer, M.; Schulze, V. The Present State of Surface Conditioning in Cutting and Grinding. *J. Manuf. Mater. Process.* **2021**, *5*, 92. [CrossRef]
25. Hao, X.; Gai, G.; Lu, F.; Zhao, X.; Zhang, Y.; Liu, J.; Yang, Y.; Gui, D.; Nan, C.-W. Dynamic mechanical properties of whisker/PA66 composites at high strain rates. *Polymer* **2005**, *46*, 3528–3534. [CrossRef]
26. Zhang, L.; Townsend, D.; Petrinic, N.; Pellegrino, A. Temperature dependent dynamic compressive response of PA66-GF30 composite under constant strain rate multiaxial loading. *Compos. Part B Eng.* **2022**, *234*, 109738. [CrossRef]